Applied Physics Express 12 (2019) 023010(4 pages), 10.7567/1882-0786/aafed5.

High critical current density $YBa_2Cu_3O_7$ coating on conductive Nb-doped $SrTiO_3$ and Ni double-buffered {100}<001> textured pure Cu tape for low-cost coated conductors without generation of any insulative oxides at interfaces

Toshiya Doi[1*], Takeo Morimura[1], Shigeru Horii[1], and Ataru Ichinose[2]

1 Graduate School of Energy Science, Kyoto University, Kyoto 605-8501, Japan
2 Central Research Institute of Electric Power Industry, Yokosuka, Kanagawa 240-0196, Japan

E-mail: doi@device.energy.kyoto-u.ac.jp

For development of a low-cost superconducting wire operating at high temperature, we propose a new approach using conductive rather than insulating buffer layers, combined with {100}<001> textured pure Cu tape to form $YBa_2Cu_3O_7$/Nb-doped $SrTiO_3$/Ni/Cu/stainless steel. The critical current density of the $YBa_2Cu_3O_7$ layer was 2.5 MA/cm^2 at 77 K in a magnetic self-field. We also confirmed that some current flowed into the Cu tape through the conductive buffer layers when the current exceeded the critical current of the $YBa_2Cu_3O_7$ layer, suggesting that the textured Cu tape worked not only as a biaxial template but also as a stabilizer layer.

Coated conductors (second generation superconducting wires, 2G-wires) become highly resistive when quenching occurs. Thus, to manufacture reliable and safe wires for high-temperature superconducting applications, it is necessary to attach conducting (metal) layers with very low resistivity to stabilize and protect the wires from damage due to quenching. Presently, insulative oxides are used for buffer layers in commercially available coated conductors. Thick Ag and Cu layers are required to be deposited as the stabilizer layers on the superconducting $REBa_2Cu_3O_7$ (REBCO; where RE represents rare-earth elements) layer. However, high costs associated with Ag and the process itself are the major obstacles for achieving low-cost 2G-wires. Use of a conductive buffer layer instead of an insulative one, combined with textured pure Cu tape, can overcome the necessity of an expensive Ag stabilizing layer for 2G-wires.

Several attempts using conductive buffers combined with {100}<001> textured pure Cu tape have been made toward exploring new architectures.[1-4)] Aytug et al. reported that they obtained a biaxially oriented $YBa_2Cu_3O_7$ (YBCO) layer on a Ni and $LaMnO_3$ (LMO) buffered Cu tape (YBCO/LMO/Ni/Cu) with sufficient critical current density (J_c) of 1×10^6 A/cm^2 at 77 K in a magnetic self-field. However, insulative NiO was formed at the interface between the LMO and Ni buffer layers (LMO/Ni interface) following LMO deposition.[1)] The J_c of a YBCO/$(La_{0.7}Sr_{0.3})MnO_3$/Ni/Cu sample was reported to be 2×10^6 A/cm^2 at 77 K in a magnetic self-field.[2)] However, insulative NiO was formed at the $(La_{0.7}Sr_{0.3})MnO_3$/Ni interface. An YBCO/(La,Sr)TiO_3/Ir/Cu structure was also attempted and the J_c was reported to be 1×10^6 A/cm^2 at 77 K in a magnetic self-field, but insulative CuO and Cu_2O were generated at the Ir/Cu or the (La, Sr)TiO_3/Ir interface.[3)] Although a number of oxides, metals, nitrides, and their combinations as the conductive buffer layers have been attempted for developing low-cost coated conductor architectures, thus far none have succeeded in fabricating a coated conductor in which the substrate Cu tape functioned as the stabilizer layer as well as the template for biaxial crystal alignment of the REBCO.

Buffer layers must exhibit at least five properties simultaneously: (1) chemical inertness to both REBCO and Cu, (2) a low diffusion coefficient for metals in the layers, (3) a low diffusion coefficient of oxygen in the layers, (4) similar lattice constants for both REBCO and Cu, and (5) low electrical resistivity. It was not easy to find a material or a combination of a few materials fulfilling the above five requirements. Due to the ease of oxidation of Cu metal tape, a very low oxygen diffusion coefficient is required for the conductive buffer material to prevent generation of insulative CuO and/or Cu_2O at the Cu/buffer interface to ensure good electrical coupling between REBCO and Cu tape.

We recently reported on the advanced architecture for an electrical self-stabilized coated conductor composed of YBCO, $Sr(Ti_{0.95}Nb_{0.05})O_3$, Ni, and Cu tape laminated with stainless steel tape (SUS316).[5, 6] Electrical resistivity of the $Sr(Ti_{0.95}Nb_{0.05})O_3$ thin film was quite low (2.5×10^{-3} Ω·cm at 77 K) and the J_c of the YBCO layer was 2.6×10^6 A/cm^2 at 77 K under a magnetic self-field for the YBCO/$Sr(Ti_{0.95}Nb_{0.05})O_3$/Ni/Cu/SUS316 tape.[5] NiO was generated at the $Sr(Ti_{0.95}Nb_{0.05})O_3$/Ni interface when the $Sr(Ti_{0.95}Nb_{0.05})O_3$ layer was 120 nm thick,[5] however, thicker $Sr(Ti_{0.95}Nb_{0.05})O_3$ layer suppressed the NiO generation.[6]

In this paper, we report the current versus voltage (*I*-*V*) characteristics near and above the critical current (I_c) and discuss electrical coupling between the YBCO layer and the Cu tape through $Sr(Ti_{0.85}Nb_{0.15})O_3$/Ni conductive buffer layers for YBCO/ $Sr(Ti_{0.85}Nb_{0.15})O_3$/Ni/Cu/SUS316 tape with a J_c of 2.5×10^6 A/cm^2.

Ni-electroplated Cu/SUS316 laminate tapes were provided from Tanaka Kikinzoku Kogyo KK as the substrates. A SUS316 tape with a thickness of 100 μm was bonded to a 30 μm thick {100}<001> textured Cu tape to strengthen the very soft annealed pure Cu tape, and a 0.5 μm thick Ni layer was electro-deposited on the surface of the laminated tape to provide Ni/Cu/SUS316 tape.[7-9] The crystal orientation of the Ni layer in the Ni/Cu/SUS316 tape was 5.0 to 5.5° (full width at half maximum (FWHM) value in the X-ray (111) ϕ-scan measurement). A Nb-doped $SrTiO_3$ (Nb-STO) thin film of 310 nm thickness was deposited in a 3% H_2/97% Ar atmosphere by a pulsed laser deposition (PLD) method using sintered bulk $Sr(Ti_{0.85}Nb_{0.15})O_{3+\delta}$ as the target. We changed the chemical composition from $Sr(Ti_{0.95}Nb_{0.05})O_{3+\delta}$, which was used in our previous works[5, 6], to $Sr(Ti_{0.85}Nb_{0.15})O_{3+\delta}$ with the objective of improving the oxygen-blocking ability of the conductive buffer layer. For deposition of Nb-STO, the chamber was maintained at 2×10^{-3} Pa pressure and with a substrate temperature of 800 °C. A 190 nm thick YBCO layer was then deposited by the PLD method in an oxygen atmosphere of 35 Pa at 740 °C, and finally annealed under oxygen flowing at 450 °C for 16 h.

The crystal orientation of the prepared sample was evaluated by X-ray diffraction measurements (θ-2θ and pole figure methods). The microstructure of the sample cross-section was observed using scanning transmission electron microscopy (STEM, JEOL JEM-2100F) with energy dispersive X-ray spectroscopy (EDX). The STEM specimens were prepared by cutting and milling using a focused ion beam. The resistivity of the Nb-STO thin film and the *I*-*V* characteristics of the specimen were measured by a standard 4-probe method. I_c was defined by an electric field criterion of 1 μV/cm. The *I*-*V* curves for YBCO/Nb-STO/Ni/Cu/SUS316 were calculated using a commercial finite element method software package “VOLT” (PHOTON Co., Ltd.) by

changing the resistivity of the Nb-STO layer in order to compare with the measured *I-V* curve.

Before Nb-STO deposition on the Ni/Cu/SUS316 tape, we prepared Nb-STO thin films on MgO(100) single crystal substrates under the same experimental conditions. The resistivity of the Nb-STO thin films were confirmed to be approximately 1.2-8.6 × 10^{-3} Ω·cm at 77 K. The Nb-STO layer was epitaxially grown on the Ni/Cu/SUS316 tape, then the YBCO thin film was deposited on the conductive Nb-STO layer. Based on the results using Nb-STO/MgO(100), the resistivity would be expected to be within the same range of 10^{-3} Ω·cm as well for Nb-STO/Ni/Cu/SUS316 tape. Figure 1 shows the (102) pole figure of the YBCO layer. Strong X-ray diffraction intensities were observed at (ψ, ϕ) = (57°, 0°), (57°, 90°), (57°, 180°), (57°, 270°) with a FWHM of 6.0° in the ϕ direction, indicating that the YBCO layer has an excellent biaxial crystal orientation. The orientation relationship between Cu, Ni, Nb-STO, and YBCO crystal was $(001)_{Cu}$ || $(001)_{Ni}$ || $(001)_{Nb\text{-}STO}$ || $(001)_{YBCO}$ and $[100]_{Cu}$ || $[100]_{Ni}$ || $[100]_{Nb\text{-}STO}$ || $[100]_{YBCO}$.

Figures 2a and 2b show bright field images (BFI) for cross-sections of the YBCO/Nb-STO/Ni/Cu/SUS316 specimen after the I_c measurement by STEM at low and high magnification, respectively. From figure 2a, no NiO or Cu oxides were observed at the interfaces of YBCO/Nb-STO, Nb-STO/Ni, or Ni/Cu over a wide area (~8 μm). We also confirmed that there were no NiO, CuO, or Cu_2O diffraction peaks in the X-ray θ-2θ spectrum for the YBCO/Nb-STO/Ni/Cu/SUS316 specimen (θ-2θ diffraction result not shown here). The vague Ni/Cu interface suggests Ni-Cu interdiffusion during the deposition of Nb-STO and YBCO. Although the grain boundary of Cu is present (figure 2a, middle-right side), the Nb-STO layer and the YBCO layer on the upper part of the figure are not subject to the grain boundary of Cu and crystal growth occurs smoothly in the direction parallel to the tape surface. When fabricating REBCO coated conductors using the RABiTS method,[10] there was a concern that the J_c may decrease owing to the existence of a groove at the grain boundaries on the surface of the metal tape like Ni-W or Cu. However, we confirmed that the groove problem does not occur in the case of the Cu tape. From figure 2b, we can see that the interfaces of YBCO/Nb-STO and Nb-STO/Ni were very sharp and clean, suggesting that the Nb-STO layer blocked both oxygen diffusion from the atmosphere through the YBCO layer to the Nb-STO/Ni interface and Ni diffusion from Ni to the YBCO layer during the YBCO deposition and oxygen annealing processes. The thickness of the YBCO and Nb-STO layers were confirmed to be 190 and 310 nm, respectively.

Figure 3 shows the BFI image and EDX elemental mapping images of Y, Ba, Cu,

Nb, Sr, O, and Ni in the same region for the cross-section of the YBCO/Nb-STO/Ni/Cu/SUS316 specimen after I_c measurement. From mapping all of the elements, it can be seen that the contrast of any element at the interfaces corresponding to YBCO, Nb-STO, and Ni layers are very clear and distinct (not vague), suggesting that the Nb-STO layer blocked the diffusion of O, Y, Ba, and Cu inward and the diffusion of Ni outward. From the mapping results of Cu and Ni, we can see that Cu diffused into the Ni layer. However, Cu did not reach the Nb-STO/Ni interface within the process time. There were no insulative NiO, CuO, nor Cu_2O species in the YBCO/Nb-STO/Ni/Cu/SUS316 specimen, that is, we can expect good electrical coupling between the YBCO layer and Cu tape through conductive Ni and Nb-STO buffer layers.

The YBCO layer of YBCO/Nb-STO/Ni/Cu/SUS316 was patterned by a Nd:YAG laser for *I-V* measurements. The distances between current tap-voltage tap and voltage tap-voltage tap were each 2 mm and the bridge width was 0.2 mm. After patterning, 200 nm thick Ag contacts were deposited on the voltage and current taps, and then the patterned YBCO/Nb-STO/Ni/Cu/SUS316 tape was annealed at 450 °C for 16 h with oxygen. Black open circles in figure 5 show the measured *I-V* characteristics of the patterned YBCO/Nb-STO/Ni/Cu/SUS316 tape immersed in liquid nitrogen in the absence of an external magnetic field. The I_c was 0.94 A, corresponding to a J_c of 2.5×10^6 A/cm^2. Red solid line in figure 5 indicates the *I-V* curve calculated using a power-law model, $V/V_0 = (I/I_0)^n$. We determined the n value to be 11.6 from the *I-V* curve of the YBCO thin films deposited on insulative $SrTiO_3$ single crystal substrates under the same experimental conditions. If the buffer layer were insulative, the measured *I-V* curve may match with the red solid line in Figure 5.

I-V curves for YBCO/Nb-STO/Ni/Cu/SUS316 were simulated by a three-dimensional finite element method (3-D FEM) by changing the resistivity of the Nb-STO layer in order to compare with the measured *I-V* curve. The potential difference between the two current taps was considered the boundary condition. In the simulation, we simplified the shape of the specimen by deleting the voltage taps, and also used the two-plane-symmetry property to reduce the FEM model to one-quarter of the original structure. The mesh size was changed gradually in the area where the change in current and/or potential is not moderate; the mesh size near the bridge and current pads was reduced to 50 nm × 70 nm × 140 nm.

Figure 6 shows the potential distribution of the meshes (a) at the bottom layer of the YBCO layer (just above the Nd-STO layer), (b) at the bottom layer of the YBCO layer near the corner of the bridge and the current tap, and (c) at the cross-sectional plane at

the center of the bridge near the corner of the bridge and the current tap, when $\rho = 1$ Ω·cm and $I = 1.9$ A. The blue color signifies that that area of the mesh is at a low potential whereas the red color signifies high potential. The black lines show the boundaries of the meshes. We confirmed that the potential distribution was reasonable by checking the gradual change of the mesh colors even near the corner of the bridge and the current tap. Gradual color change from red to blue from the YBCO layer toward the Ni layer in figure 6 (c) indicates that some portion of the current flowing in the YBCO layer goes into the Ni layer through the Nb-STO layer. Before plotting the *I-V* curve, for all the FEM calculation cases, the potentials and current vectors for all meshes were confirmed to be reasonable. *I* was the total current in the specimen and *V* was the potential difference between the two voltage taps; these correspond to the measured *I* and *V*, respectively. In the 3D-FEM calculation, we applied $V/V_0 = (I/I_0)^{11.6}$ to the *I-V* characteristics of the YBCO layer. The resistivities of Ag, Ni, Cu, and SUS316 were fixed at 0.2, 0.55, 0.2, and 55 μΩ·cm (resistivities at 77 K), respectively, and the resistivity (ρ) of Nb-STO was swept from 1×10^{-3} to 1×10^{3} Ω·cm. We confirmed that the simulated *I-V* curves approach that calculated by the power-law model with increasing ρ, and that the *I-V* curves approach a straight line expressed by the equation $V=\rho_{Cu} \times (I - I_c)$ in the $I > I_c$ region with decreasing ρ, where ρ_{Cu} is the resistivity of Cu.

In Figure 5, the blue triangles ($\rho = 1$ Ω·cm), light blue squares ($\rho = 5$ Ω·cm), green diamonds ($\rho = 10$ Ω·cm), and orange pentagons ($\rho = 100$ Ω·cm) represent the values calculated by 3-D FEM. The experimental data resides between the calculated *I-V* curves of 1 Ω·cm and 5 Ω·cm, clearly showing that some current flowed into the Cu tape through the conductive Nb-STO and Ni buffer layers in $I > I_c$ regions, that is, {100}<001> textured pure Cu tape functioned as the stabilizer layer as well as the template for YBCO biaxial crystal alignment.

Although the resistivity of Nb-STO was previously assumed to be approximately $1.2\text{-}8.6 \times 10^{-3}$ Ω·cm at 77 K, after YBCO deposition and oxygen annealing, the resistivity was estimated from figure 5 to be a few Ω·cm. Because an oxygen vacancy in STO forms a donor center[11], increasing the oxygen content of Nb-STO also increases the resistivity. The observed increase in resistivity of the Nb-STO layer suggests that oxygen diffused into the Nb-STO layer through the YBCO layer from the atmosphere during the YBCO deposition and oxygen annealing processes. The lower ρ of the conductive buffer layer apparently provides a shorter current transfer length. Efforts toward finding more effective oxygen-blocking materials with low resistivity are the next step to further improve this system. Discovering more effective oxygen-blocking materials with low resistivity is underway.

In conclusion, we demonstrated that the {100}<001> textured pure Cu tape worked not only as the template for YBCO biaxial crystal alignment but also as the stabilizer layer for the newly coated conductor architecture of the YBCO/Nb-STO/Ni/Cu/SUS316 tape. The interfaces of YBCO/Nb-STO and Nb-STO/Ni were very sharp and clean, and no NiO, CuO, nor Cu_2O species were generated in our coated conductor utilizing a new buffer layer approach. From comparison of the measured and calculated *I-V* characteristics, it was confirmed that some current flowed into the Cu tape from the YBCO layer through conductive Nb-STO and Ni buffer layers in $I > I_c$ regions. The J_c at 77 K in a magnetic self-field was 2.5×10^6 A/cm^2, making this the first example whereby incorporation of a conductive buffer layer for a coated conductor not only functions, but also results in a commercially competitive J_c. We believe that our architecture may provide a new way to realize low-cost and commercially feasible coated conductors.

Acknowledgements
A part of this work was supported by JST ALCA Grant Number JPMJAL1109, Japan.

References

1) T. Aytug, A. Goyal, N. Rutter, M. Paranthaman, J.R. Thompson, H.Y. Zhai, and D.K. Christen, J. Mater. Res. **18**, 872 (2003).
2) T. Aytug, M. Paranthaman, J. R. Thompson, A. Goyal, N. Rutter, H. Y. Zhai, A. A. Gapud, A. O. Ijaduola, and D. K. Christen, Appl. Phys. Lett. **83**, 3963 (2003).
3) K. Kim, D.P. Norton, C. Cantoni, T. Aytug, A.A. Gapud, M.P. Paranthaman, A. Goyal, and D.K. Christen, IEEE Trans. Appl. Supercond. **15**, 2997 (2005).
4) K. Kim, M. Paranthaman, D.P. Norton, T. Aytug, C. Cantoni, A.A. Gapud, A. Goyal, and D.K. Christen, Supercond. Sci. Technol. **19**, R23 (2006).
5) T. Doi, M. Hashimoto, S. Horii, and A. Ichinose, Mater. Trans. **58**, 1493 (2017).
6) A. Ichinose, S. Horii, and T. Doi, Jpn. J. Appl. Phys. **56**, 103101 (2017).
7) M. Tokudome, T. Doi, R. Tomiyasu, M. Daio, Y. Hakuraku, K. Shima, S. Kubota, N. Kashima, and S. Nagaya, IEEE Trans. Appl. Supercond. **19**, 3287 (2009).
8) N. Kashima, K. Shima, T. Doi, S. Kubota, T. Watanabe, M. Inoue, T. Kiss, and S. Nagaya, IEEE Trans. Appl. Supercond. **19**, 3299 (2009).
9) N. Kashima, S. Kubota, K. Shima, T. Doi, S. Nagaya, M. Inoue, and T. Kiss, Jpn. J. Appl. Phys. **50**, 063101 (2011).
10) A. Goyal, D.P. Norton, J.D. Budai, M. Paranthaman, E.D. Specht, D.M. Kroeger, D.K. Christen, Q. He, B. Saffian, F.A. List, D.F. Lee, P.M. Martin, C.E. Klabunde, E. Hartfield, and V.K. Sikka, Appl. Phys. Lett. **69**, 1795 (1996).
11) O. N. Tufte and P. W. Chapman, Phys. Rev. **155**, 196(1967).

Figure captions

Figure 1

X-ray $(102)_{YBCO}$ pole figure for an YBCO/Nb-STO/Ni/Cu/SUS316 specimen.

Figure 2

Cross-sectional STEM images of the YBCO/Nb-STO/Ni/Cu/SUS316 tape at (a) low and (b) high magnifications.

Figure 3

STEM image and EDX mapping images of Y, Ba, Cu, Nb, Sr, O, and Ni in the same region as the cross-section of the YBCO/Nb-STO/Ni/Cu/SUS316 specimen.

Figure 4

Schematic of the patterned YBCO/Nb-STO/Ni/Cu/SUS316 sample.

Figure 5

Current versus voltage curves of the YBCO/Nb-STO/Ni/Cu/SUS316 specimen measured in liquid nitrogen without external magnetic field (black open circle), the calculated data in cases of ρ = 1 (blue solid triangle), 5 (light blue solid square), 10 (green solid diamond), 100 Ω·cm (orange solid pentagon) by a FEM, and the calculated curve (red solid line) using a power-low model with n = 11.6.

Figure 6

Potential distribution of the meshes (a) at the bottom layer of the YBCO layer (just above the Nd-STO layer), (b) at the bottom layer of the YBCO layer near the corner of the bridge and the current tap, and (c) at the cross-sectional plane at the center of the bridge near the corner of the bridge and the current tap.

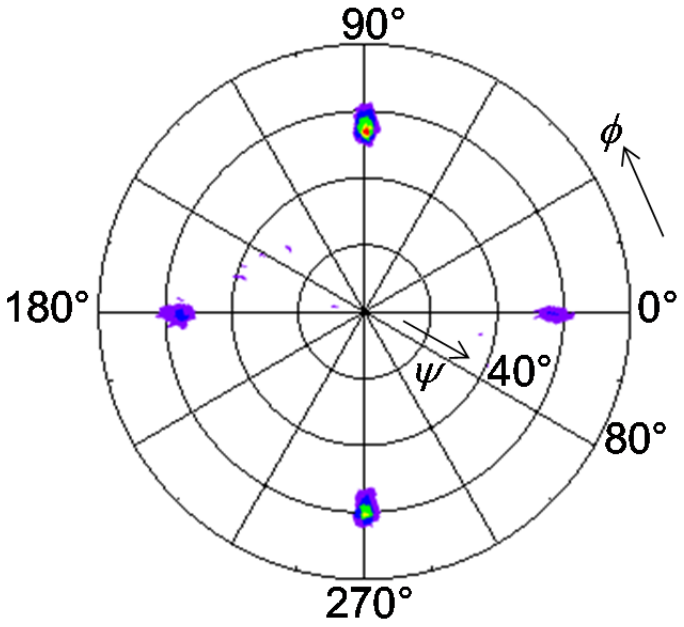

Fig.1.

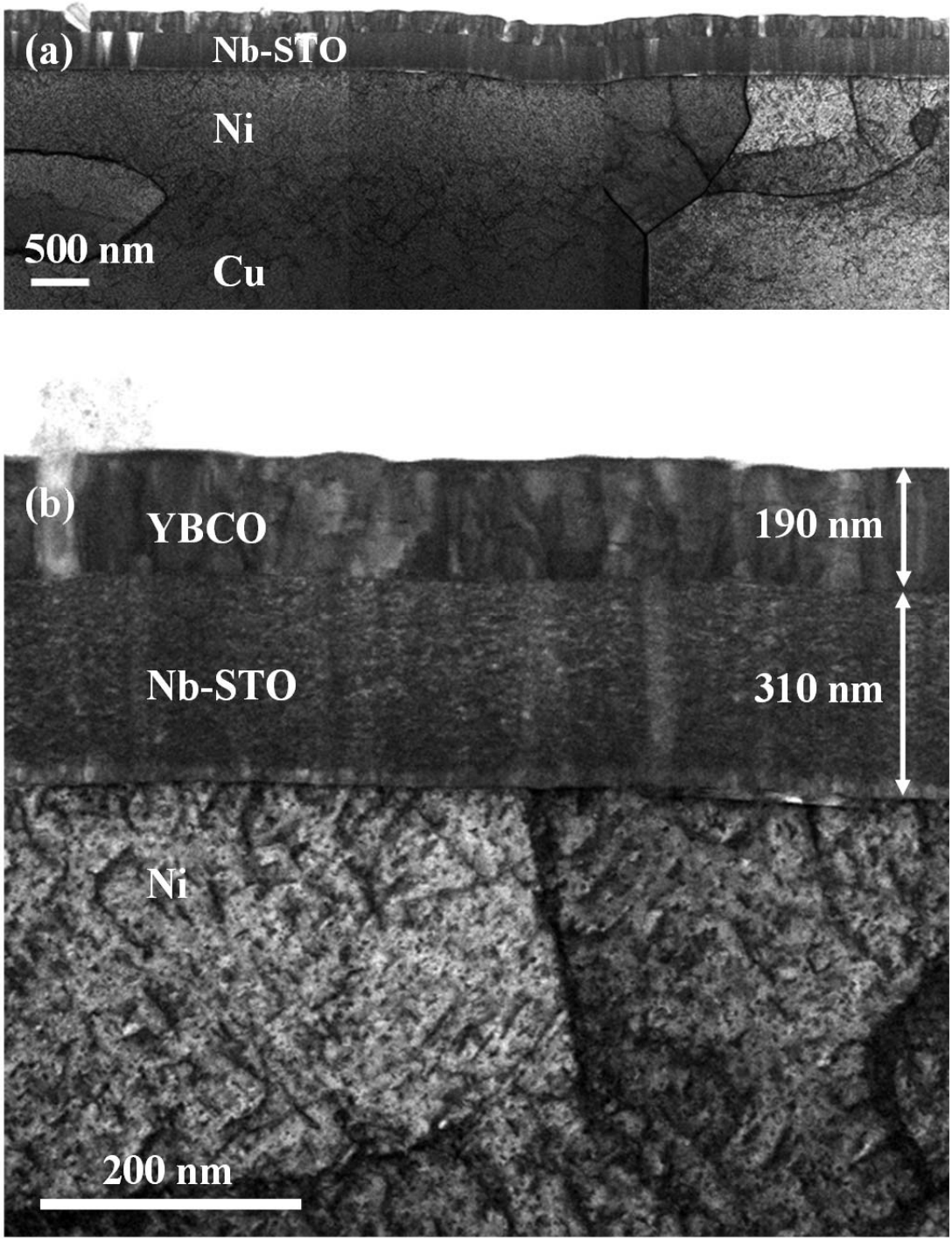

Fig.2.

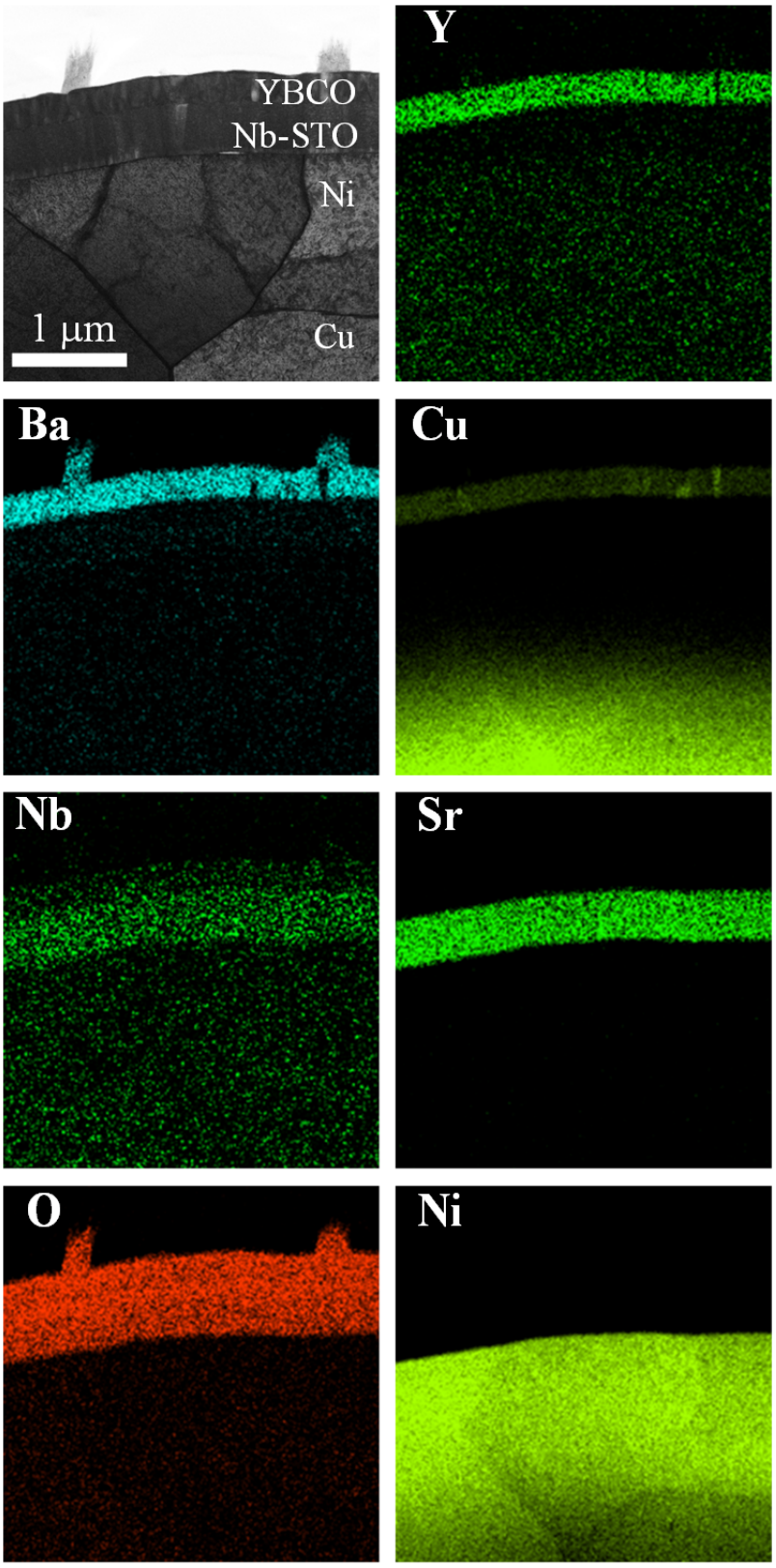

Fig.3.

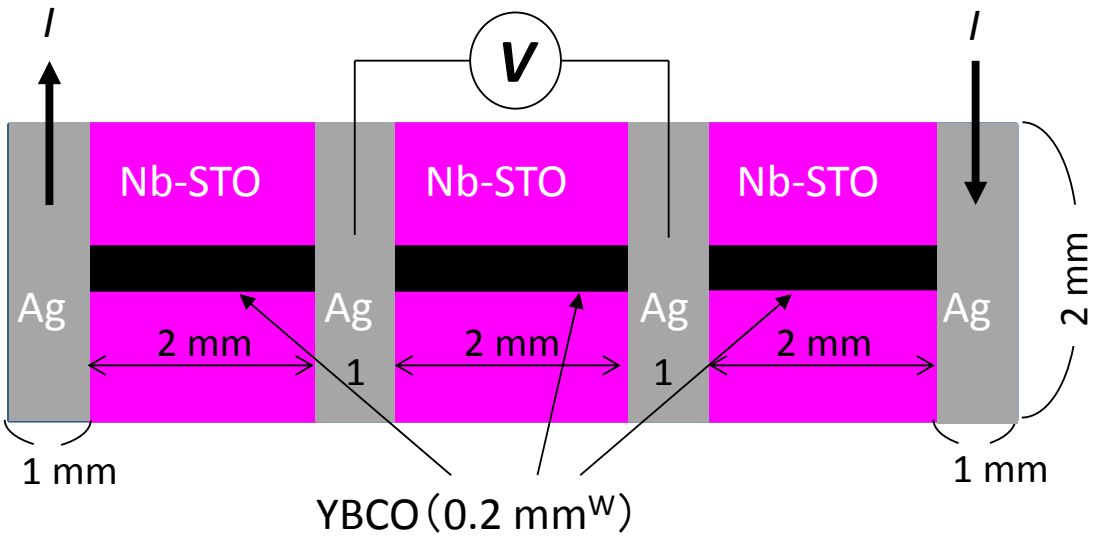
I
V
I
Nb-STO
Nb-STO
Nb-STO
Ag
Ag
Ag
Ag
2 mm
2 mm
2 mm
1
1
2 mm
1 mm
1 mm
YBCO（0.2 mmW）

Fig.4.

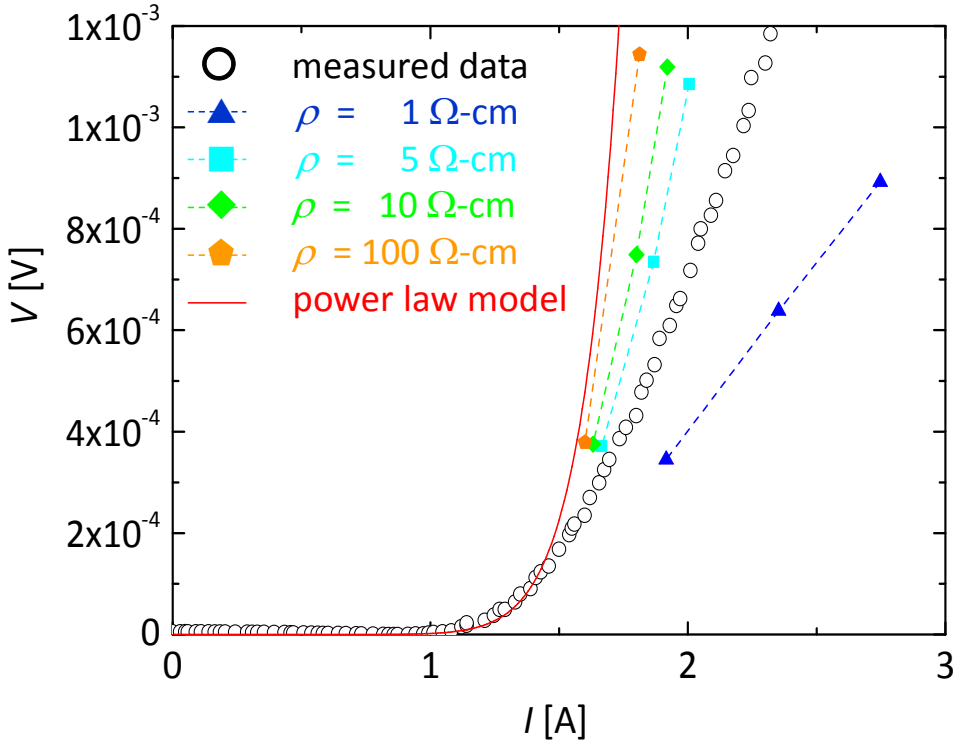
1x10-3
1x10-3
8x10-4
6x10-4
4x10-4
2x10-4
0
V [V]
0
1
2
3
I [A]
measured data
ρ = 1 Ω-cm
ρ = 5 Ω-cm
ρ = 10 Ω-cm
ρ = 100 Ω-cm
power law model

Fig.5.

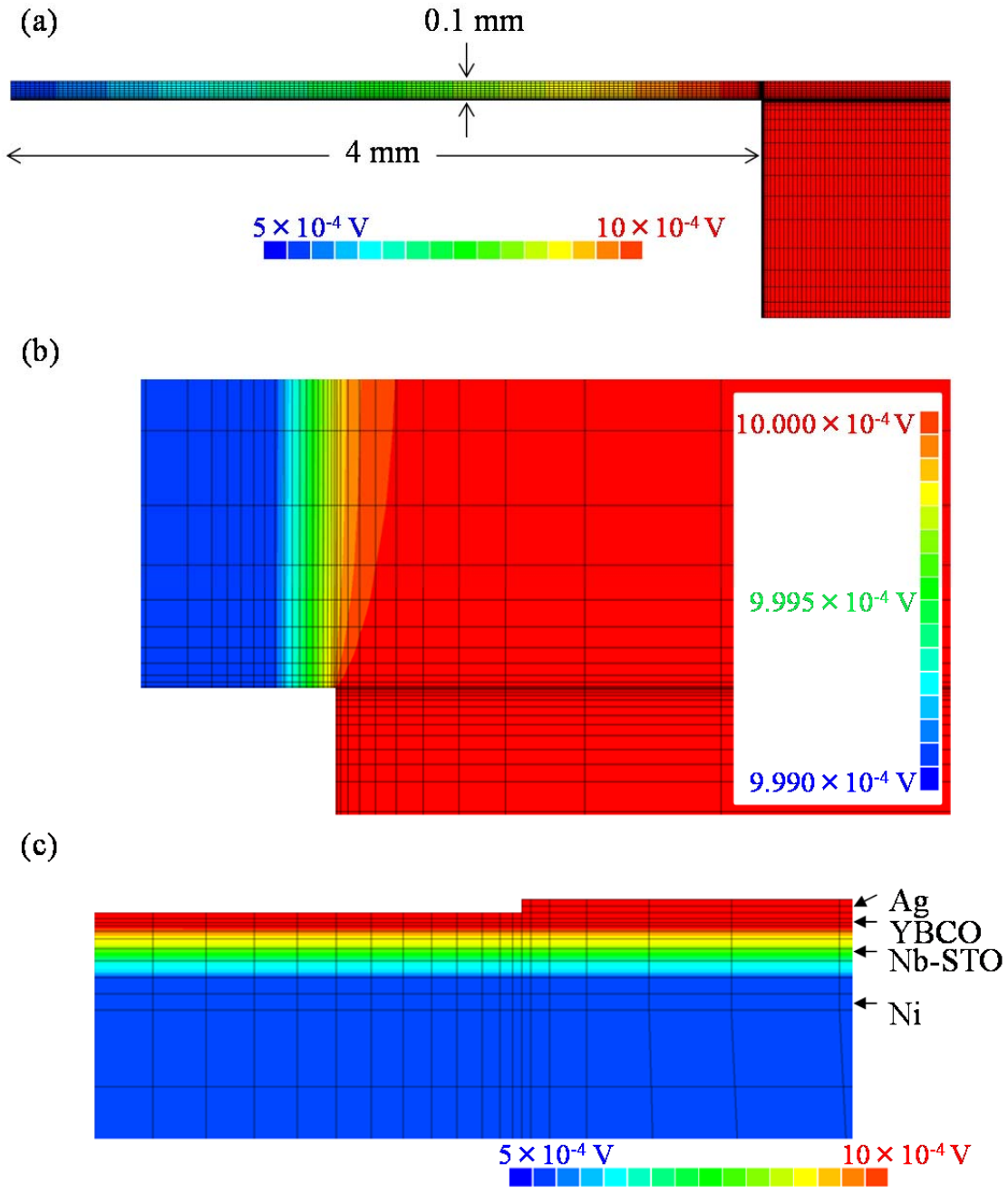
(a)
0.1 mm
4 mm
5 × 10-4 V
10 × 10-4 V
(b)
10.000 × 10-4 V
9.995 × 10-4 V
9.990 × 10-4 V
(c)
Ag
YBCO
Nb-STO
Ni
5 × 10-4 V
10 × 10-4 V

Fig.6.